

DESY 98-018
February 1998

High- E_T Inclusive Jet Cross Sections in Photoproduction at HERA

ZEUS Collaboration

Abstract

Inclusive jet differential cross sections for the reaction $e^+p \rightarrow e^+ + \text{jet} + X$ with quasi-real photons have been measured with the ZEUS detector at HERA. These cross sections are given for the photon-proton centre-of-mass energy interval $134 < W < 277$ GeV and jet pseudorapidity in the range $-1 < \eta^{jet} < 2$ in the laboratory frame. The results are presented for three cone radii in the $\eta - \varphi$ plane, $R = 1.0, 0.7$ and 0.5 . Measurements of $d\sigma/d\eta^{jet}$ above various jet-transverse-energy thresholds up to 25 GeV and in three ranges of W are presented and compared to next-to-leading order (NLO) QCD calculations. For jets defined with $R = 1.0$ differences between data and NLO calculations are seen at high η^{jet} and low E_T^{jet} . The measured cross sections for jets defined with $R = 0.7$ are well described by the calculations in the entire measured range of η^{jet} and E_T^{jet} . The inclusive jet cross section for $E_T^{jet} > 21$ GeV is consistent with an approximately linear variation with the cone radius R in the range between 0.5 and 1.0, and with NLO calculations.

arXiv:hep-ex/9802012v1 12 Feb 1998

The ZEUS Collaboration

J. Breitweg, M. Derrick, D. Krakauer, S. Magill, D. Mikunas, B. Musgrave, J. Repond, R. Stanek,
R.L. Talaga, R. Yoshida, H. Zhang
Argonne National Laboratory, Argonne, IL, USA ^p

M.C.K. Mattingly
Andrews University, Berrien Springs, MI, USA

F. Anselmo, P. Antonioli, G. Bari, M. Basile, L. Bellagamba, D. Boscherini, A. Bruni, G. Bruni,
G. Cara Romeo, G. Castellini¹, L. Cifarelli², F. Cindolo, A. Contin, M. Corradi, S. De Pasquale,
I. Gialas³, P. Giusti, G. Iacobucci, G. Laurenti, G. Levi, A. Margotti, T. Massam, R. Nania,
F. Palmonari, A. Pesci, A. Polini, F. Ricci, G. Sartorelli, Y. Zamora Garcia⁴, A. Zichichi
University and INFN Bologna, Bologna, Italy ^f

C. Amelung, A. Bornheim, I. Brock, K. Coböken, J. Crittenden, R. Deffner, M. Eckert,
M. Grothe, H. Hartmann, K. Heinloth, L. Heinz, E. Hilger, H.-P. Jakob, A. Kappes, U.F. Katz,
R. Kerger, E. Paul, M. Pfeiffer, J. Stamm⁵, R. Wedemeyer⁶, H. Wieber
Physikalisches Institut der Universität Bonn, Bonn, Germany ^c

D.S. Bailey, S. Campbell-Robson, W.N. Cottingham, B. Foster, R. Hall-Wilton, G.P. Heath,
H.F. Heath, J.D. McFall, D. Piccioni, D.G. Roff, R.J. Tapper
H.H. Wills Physics Laboratory, University of Bristol, Bristol, U.K. ^o

R. Ayad, M. Capua, A. Garfagnini, L. Iannotti, M. Schioppa, G. Susinno
Calabria University, Physics Dept.and INFN, Cosenza, Italy ^f

J.Y. Kim, J.H. Lee, I.T. Lim, M.Y. Pac⁷
Chonnam National University, Kwangju, Korea ^h

A. Caldwell⁸, N. Cartiglia, Z. Jing, W. Liu, B. Mellado, J.A. Parsons, S. Ritz⁹, S. Sampson,
F. Sciulli, P.B. Straub, Q. Zhu
Columbia University, Nevis Labs., Irvington on Hudson, N.Y., USA ^q

P. Borzemeski, J. Chwastowski, A. Eskreys, J. Figiel, K. Klimek, M.B. Przybycień, L. Zawiejski
Inst. of Nuclear Physics, Cracow, Poland ^j

L. Adamczyk¹⁰, B. Bednarek, M. Bukowy, A. Czermak, K. Jeleń, D. Kisielewska, T. Kowalski,
M. Przybycień, E. Rulikowska-Zarebska, L. Suszycki, J. Zając
Faculty of Physics and Nuclear Techniques, Academy of Mining and Metallurgy, Cracow, Poland ^j

Z. Duliński, A. Kotański
Jagellonian Univ., Dept. of Physics, Cracow, Poland ^k

G. Abbiendi¹¹, L.A.T. Bauerdick, U. Behrens, H. Beier, J.K. Bienlein, G. Cases¹², K. Desler,
G. Drews, U. Fricke, F. Goebel, P. Göttlicher, R. Graciani, T. Haas, W. Hain, D. Hasell,
K. Hebbel, K.F. Johnson¹³, M. Kasemann, W. Koch, U. Kötz, H. Kowalski, L. Lindemann,
B. Löhr, J. Milewski, T. Monteiro¹⁴, J.S.T. Ng¹⁵, D. Notz, I.H. Park¹⁶, A. Pellegrino,
F. Pelucchi, K. Piotrkowski, M. Rohde, J. Roldán¹⁷, J.J. Ryan¹⁸, A.A. Savin, U. Schneekloth,
O. Schwarzer, F. Selonke, B. Surov, E. Tassi, D. Westphal, G. Wolf, U. Wollmer, C. Youngman,
W. Zeuner
Deutsches Elektronen-Synchrotron DESY, Hamburg, Germany

B.D. Burow, C. Coldewey, H.J. Grabosch, A. Meyer, S. Schlenstedt
DESY-IfH Zeuthen, Zeuthen, Germany

G. Barbagli, E. Gallo, P. Pelfer
University and INFN, Florence, Italy^f

G. Maccarrone, L. Votano
INFN, Laboratori Nazionali di Frascati, Frascati, Italy^f

A. Bamberger, S. Eisenhardt, P. Markun, T. Trefzger¹⁹, S. Wölflé
Fakultät für Physik der Universität Freiburg i.Br., Freiburg i.Br., Germany^c

J.T. Bromley, N.H. Brook, P.J. Bussey, A.T. Doyle²⁰, N. Macdonald, D.H. Saxon, L.E. Sinclair,
E. Strickland, R. Waugh
Dept. of Physics and Astronomy, University of Glasgow, Glasgow, U.K.^o

I. Bohnet, N. Gendner, U. Holm, A. Meyer-Larsen, H. Salehi, K. Wick
Hamburg University, I. Institute of Exp. Physics, Hamburg, Germany^c

L.K. Gladilin²¹, D. Horstmann, D. Kçira²², R. Klanner, E. Lohrmann, G. Poelz, W. Schott¹⁸,
F. Zetsche
Hamburg University, II. Institute of Exp. Physics, Hamburg, Germany^c

T.C. Bacon, I. Butterworth, J.E. Cole, G. Howell, L. Lamberti²³, K.R. Long, D.B. Miller,
N. Pavel, A. Priniyas²⁴, J.K. Sedgbeer, D. Sideris, R. Walker
Imperial College London, High Energy Nuclear Physics Group, London, U.K.^o

U. Mallik, S.M. Wang, J.T. Wu
University of Iowa, Physics and Astronomy Dept., Iowa City, USA^p

P. Cloth, D. Filges
Forschungszentrum Jülich, Institut für Kernphysik, Jülich, Germany

J.I. Fleck²⁵, T. Ishii, M. Kuze, I. Suzuki²⁶, K. Tokushuku, S. Yamada, K. Yamauchi, Y. Yamazaki²⁷
Institute of Particle and Nuclear Studies, KEK, Tsukuba, Japan^g

S.J. Hong, S.B. Lee, S.W. Nam²⁸, S.K. Park
Korea University, Seoul, Korea^h

F. Barreiro, J.P. Fernández, G. García, C. Glasman²⁹, J.M. Hernández, L. Hervás²⁵, L. Labarga,
M. Martínez, J. del Peso, J. Puga, J. Terrón, J.F. de Trocóniz
Univer. Autónoma Madrid, Depto de Física Teórica, Madrid, Spainⁿ

F. Corriveau, D.S. Hanna, J. Hartmann, L.W. Hung, W.N. Murray, A. Ochs, M. Riveline,
D.G. Stairs, M. St-Laurent, R. Ullmann
McGill University, Dept. of Physics, Montréal, Québec, Canada^{a, b}

T. Tsurugai
Meiji Gakuin University, Faculty of General Education, Yokohama, Japan

V. Bashkirov, B.A. Dolgoshein, A. Stifutkin
Moscow Engineering Physics Institute, Moscow, Russia^l

G.L. Bashindzhagyan, P.F. Ermolov, Yu.A. Golubkov, L.A. Khein, N.A. Korotkova,
I.A. Korzhavina, V.A. Kuzmin, O.Yu. Lukina, A.S. Proskuryakov, L.M. Shcheglova³⁰,
A.N. Solomin³⁰, S.A. Zotkin

Moscow State University, Institute of Nuclear Physics, Moscow, Russia^m

C. Bokel, M. Botje, N. Brümmer, J. Engelen, E. Koffeman, P. Kooijman, A. van Sighem,
H. Tiecke, N. Tuning, W. Verkerke, J. Vosseveld, L. Wiggers, E. de Wolf

NIKHEF and University of Amsterdam, Amsterdam, Netherlandsⁱ

D. Acosta³¹, B. Bylsma, L.S. Durkin, J. Gilmore, C.M. Ginsburg, C.L. Kim, T.Y. Ling,
P. Nylander, T.A. Romanowski³²

Ohio State University, Physics Department, Columbus, Ohio, USA^p

H.E. Blaikley, R.J. Cashmore, A.M. Cooper-Sarkar, R.C.E. Devenish, J.K. Edmonds,
J. Große-Knetter³³, N. Harnew, C. Nath, V.A. Noyes³⁴, A. Quadt, O. Ruske, J.R. Tickner²⁴,
H. Uijterwaal, R. Walczak, D.S. Waters

Department of Physics, University of Oxford, Oxford, U.K.^o

A. Bertolin, R. Brugnera, R. Carlin, F. Dal Corso, U. Dosselli, S. Limentani, M. Morandin,
M. Posocco, L. Stanco, R. Stroili, C. Voci

Dipartimento di Fisica dell' Università and INFN, Padova, Italy^f

J. Bulmahn, B.Y. Oh, J.R. Okrasinski, W.S. Toothacker, J.J. Whitmore

Pennsylvania State University, Dept. of Physics, University Park, PA, USA^q

Y. Iga

Polytechnic University, Sagamihara, Japan^g

G. D'Agostini, G. Marini, A. Nigro, M. Raso

Dipartimento di Fisica, Univ. 'La Sapienza' and INFN, Rome, Italy^f

J.C. Hart, N.A. McCubbin, T.P. Shah

Rutherford Appleton Laboratory, Chilton, Didcot, Oxon, U.K.^o

D. Epperson, C. Heusch, J.T. Rahn, H.F.-W. Sadrozinski, A. Seiden, R. Wichmann, D.C. Williams
University of California, Santa Cruz, CA, USA^p

H. Abramowicz³⁵, G. Briskin, S. Dagan³⁶, S. Kananov³⁶, A. Levy³⁶

*Raymond and Beverly Sackler Faculty of Exact Sciences, School of Physics, Tel-Aviv University,
Tel-Aviv, Israel^e*

T. Abe, T. Fusayasu, M. Inuzuka, K. Nagano, K. Umemori, T. Yamashita

Department of Physics, University of Tokyo, Tokyo, Japan^g

R. Hamatsu, T. Hirose, K. Homma³⁷, S. Kitamura³⁸, T. Matsushita

Tokyo Metropolitan University, Dept. of Physics, Tokyo, Japan^g

M. Arneodo, R. Cirio, M. Costa, M.I. Ferrero, S. Maselli, V. Monaco, C. Peroni, M.C. Petrucci,
M. Ruspa, R. Sacchi, A. Solano, A. Staiano

Università di Torino, Dipartimento di Fisica Sperimentale and INFN, Torino, Italy^f

M. Dardo

II Faculty of Sciences, Torino University and INFN - Alessandria, Italy^f

D.C. Bailey, C.-P. Fagerstroem, R. Galea, G.F. Hartner, K.K. Joo, G.M. Levman, J.F. Martin, R.S. Orr, S. Polenz, A. Sabetfakhri, D. Simmons, R.J. Teuscher²⁵
University of Toronto, Dept. of Physics, Toronto, Ont., Canada^a

J.M. Butterworth, C.D. Catterall, M.E. Hayes, T.W. Jones, J.B. Lane, R.L. Saunders, M.R. Sutton, M. Wing
University College London, Physics and Astronomy Dept., London, U.K.^o

J. Ciborowski, G. Grzelak³⁹, M. Kasprzak, R.J. Nowak, J.M. Pawlak, R. Pawlak, T. Tymieniecka, A.K. Wróblewski, J.A. Zakrzewski, A.F. Żarnecki
Warsaw University, Institute of Experimental Physics, Warsaw, Poland^j

M. Adamus
Institute for Nuclear Studies, Warsaw, Poland^j

O. Deppe, Y. Eisenberg³⁶, D. Hochman, U. Karshon³⁶
Weizmann Institute, Department of Particle Physics, Rehovot, Israel^d

W.F. Badgett, D. Chapin, R. Cross, S. Dasu, C. Foudas, R.J. Loveless, S. Mattingly, D.D. Reeder, W.H. Smith, A. Vaiciulis, M. Wodarczyk
University of Wisconsin, Dept. of Physics, Madison, WI, USA^p

A. Deshpande, S. Dhawan, V.W. Hughes
Yale University, Department of Physics, New Haven, CT, USA^p

S. Bhadra, W.R. Frisken, M. Khakzad, W.B. Schmidke
York University, Dept. of Physics, North York, Ont., Canada^a

¹ also at IROE Florence, Italy
² now at Univ. of Salerno and INFN Napoli, Italy
³ now at Univ. of Crete, Greece
⁴ supported by Worldlab, Lausanne, Switzerland
⁵ now at C. Plath GmbH, Hamburg
⁶ retired
⁷ now at Dongshin University, Naju, Korea
⁸ also at DESY
⁹ Alfred P. Sloan Foundation Fellow
¹⁰ supported by the Polish State Committee for Scientific Research, grant No. 2P03B14912
¹¹ now at INFN Bologna
¹² now at SAP A.G., Walldorf
¹³ visitor from Florida State University
¹⁴ supported by European Community Program PRAXIS XXI
¹⁵ now at DESY-Group FDET
¹⁶ visitor from Kyungpook National University, Taegu, Korea, partially supported by DESY
¹⁷ now at IFIC, Valencia, Spain
¹⁸ now a self-employed consultant
¹⁹ now at ATLAS Collaboration, Univ. of Munich
²⁰ also at DESY and Alexander von Humboldt Fellow at University of Hamburg
²¹ on leave from MSU, supported by the GIF, contract I-0444-176.07/95
²² supported by DAAD, Bonn
²³ supported by an EC fellowship
²⁴ PPARC Post-doctoral Fellow
²⁵ now at CERN
²⁶ now at Osaka Univ., Osaka, Japan
²⁷ supported by JSPS Postdoctoral Fellowships for Research Abroad
²⁸ now at Wayne State University, Detroit
²⁹ supported by an EC fellowship number ERBFMBICT 972523
³⁰ partially supported by the Foundation for German-Russian Collaboration DFG-RFBR
(grant no. 436 RUS 113/248/3 and no. 436 RUS 113/248/2)
³¹ now at University of Florida, Gainesville, FL, USA
³² now at Department of Energy, Washington
³³ supported by the Feodor Lynen Program of the Alexander von Humboldt foundation
³⁴ Glasstone Fellow
³⁵ an Alexander von Humboldt Fellow at University of Hamburg
³⁶ supported by a MINERVA Fellowship
³⁷ now at ICEPP, Univ. of Tokyo, Tokyo, Japan
³⁸ present address: Tokyo Metropolitan College of Allied Medical Sciences, Tokyo 116, Japan
³⁹ supported by the Polish State Committee for Scientific Research, grant No. 2P03B09308

- a* supported by the Natural Sciences and Engineering Research Council of Canada (NSERC)
- b* supported by the FCAR of Québec, Canada
- c* supported by the German Federal Ministry for Education and Science, Research and Technology (BMBF), under contract numbers 057BN19P, 057FR19P, 057HH19P, 057HH29P
- d* supported by the MINERVA Gesellschaft für Forschung GmbH, the German Israeli Foundation, and the U.S.-Israel Binational Science Foundation
- e* supported by the German-Israeli Foundation, the Israel Science Foundation, the U.S.-Israel Binational Science Foundation, and by the Israel Ministry of Science
- f* supported by the Italian National Institute for Nuclear Physics (INFN)
- g* supported by the Japanese Ministry of Education, Science and Culture (the Monbusho) and its grants for Scientific Research
- h* supported by the Korean Ministry of Education and Korea Science and Engineering Foundation
- i* supported by the Netherlands Foundation for Research on Matter (FOM)
- j* supported by the Polish State Committee for Scientific Research, grant No. 115/E-343/SPUB/P03/002/97, 2P03B10512, 2P03B10612, 2P03B14212, 2P03B10412
- k* supported by the Polish State Committee for Scientific Research (grant No. 2P03B08308) and Foundation for Polish-German Collaboration
- l* partially supported by the German Federal Ministry for Education and Science, Research and Technology (BMBF)
- m* supported by the Fund for Fundamental Research of Russian Ministry for Science and Education and by the German Federal Ministry for Education and Science, Research and Technology (BMBF)
- n* supported by the Spanish Ministry of Education and Science through funds provided by CICYT
- o* supported by the Particle Physics and Astronomy Research Council
- p* supported by the US Department of Energy
- q* supported by the US National Science Foundation

1 Introduction

At HERA, photon-proton reactions are studied by means of ep scattering at low four-momentum transfers squared ($Q^2 \approx 0$). In photoproduction, two types of QCD processes contribute to the production of jets [1, 2] at leading order (LO): either the photon interacts directly with a parton in the proton (the direct process) or the photon acts as a source of partons which interact with those in the proton (the resolved process). Differential cross sections for inclusive jet photoproduction using a cone algorithm have been previously presented as a function of the jet pseudorapidity¹ (η^{jet}) and transverse energy (E_T^{jet}) for E_T^{jet} up to 17 GeV [3, 4, 5]. The calculated cross sections depend on the proton parton distributions in the region of Bjorken- x above approximately 10^{-2} , where they are well constrained by other measurements [6]. Such jet measurements therefore offer a potential means of studying the parton distributions in the photon [2, 7, 8, 9, 10, 11] at higher scales than those probed in e^+e^- interactions [12]. However, various aspects of the comparison between theory and experiment need to be addressed before a reliable determination of the photon parton distributions can be made.

Next-to-leading order (NLO) calculations including resolved plus direct processes and using the NLO parametrisations of the photon parton distributions of GRV [13] have been compared [8] to our previous measurements [4]. Discrepancies were observed in the forward region ($\eta^{jet} > 1$) for low E_T^{jet} ($E_T^{jet} \sim 8$ GeV) which prevented any strong conclusion being drawn on the photon parton distributions. Moreover, the comparison of the transverse energy flow between data and leading-logarithm parton-shower Monte Carlo simulations [4] showed a discrepancy at high η^{jet} that could be attributed to energy not associated with the hard-scattering process (the ‘underlying event’). Such an underlying event is not included in the NLO calculations and, therefore, the comparison between data and NLO calculations becomes problematic. The transverse energy inside the cone of the jet in the $\eta - \varphi$ plane due to the underlying event is naively expected to be proportional to the area covered by the cone. Therefore, measurements performed with different cone radii can elucidate the effects of a possible underlying event. In addition, the NLO calculations for jets defined with a cone radius $R \approx 0.7$ are expected to be most stable with respect to variations of the renormalisation and factorisation scales [14]. Measurements of the jet cross sections in different ranges of the γp centre-of-mass energy (W) provide a further means of comparing data and calculations.

In this paper, measurements of $d\sigma/d\eta^{jet}$ are presented for various cone radii. In each case, measurements of $d\sigma/d\eta^{jet}$ integrated above four different E_T^{jet} thresholds (14, 17, 21 and 25 GeV) are performed. For $R = 1.0$, the measurement of $d\sigma/d\eta^{jet}$ is extended to higher E_T^{jet} values as compared to the previous data [4]. We have, in addition, a better understanding of the energy scale of the jets. First measurements of $d\sigma/d\eta^{jet}$ in three regions of W are presented for $R = 1.0$ and 0.7. The dependence of the inclusive jet cross section on the jet cone radius is presented. NLO calculations [9, 10] which include resolved plus direct processes are compared to the measurements.

The data sample used in this analysis was collected with the ZEUS detector in e^+p interactions at the HERA collider and corresponds to an integrated luminosity of 2.65 pb^{-1} , which is a five-fold increase in statistics over the previous analysis [4].

¹The ZEUS coordinate system is defined as right-handed with the Z axis pointing in the proton beam direction, hereafter referred to as forward, and the X axis horizontal, pointing towards the centre of HERA. The pseudorapidity is defined as $\eta = -\ln(\tan \frac{\theta}{2})$, where the polar angle θ is taken with respect to the proton beam direction.

2 Experimental conditions

During 1994 HERA operated with protons of energy $E_p = 820$ GeV and positrons of energy $E_e = 27.5$ GeV. The ZEUS detector is described in detail in [15, 16]. The main subdetectors used in the present analysis are the central tracking system positioned in a 1.43 T solenoidal magnetic field and the uranium-scintillator sampling calorimeter (CAL). The tracking system was used to establish an interaction vertex and to cross-check the energy scale of the CAL. Energy deposits in the CAL were used in the jet finding and to measure jet energies. The CAL is hermetic and consists of 5918 cells each read out by two photomultiplier tubes. Under test beam conditions, the CAL has energy resolutions of $18\%/\sqrt{E}$ for electrons and $35\%/\sqrt{E}$ for hadrons. Jet energies are corrected for the energy lost in inactive material in front of the CAL which is typically about one radiation length (see Section 5). The effects of uranium noise were minimised by discarding cells in the inner (electromagnetic) or outer (hadronic) sections if they had energy deposits of less than 60 MeV or 110 MeV, respectively. The luminosity was measured from the rate of the bremsstrahlung process $e^+p \rightarrow e^+p\gamma$. A three-level trigger was used to select events online [16, 17].

3 Data selection and jet search

Offline, events from quasi-real photon-proton collisions were selected using similar criteria as employed previously [4]. The main steps are briefly discussed here. The contamination from beam-gas interactions, cosmic showers and beam-halo muons is negligible after demanding: a) at least two tracks pointing to the vertex; b) the vertex position along the beam axis to lie in the range $-29 < Z < 36$ cm; c) fewer than five tracks not associated with the vertex and compatible with an interaction upstream in the direction of the proton beam; and d) the number of tracks not associated to the vertex be less than 10% of the total number of tracks. Deep-inelastic (DIS) charged-current e^+p scattering events are rejected by requiring the total missing transverse momentum (p_T) to be small compared to the total transverse energy (E_T^{tot}): $p_T/\sqrt{E_T^{tot}} < 2$ GeV $^{1/2}$. DIS neutral-current events with an identified scattered positron candidate in the CAL, according to the algorithm described in [18], are removed from the sample. The selected sample consists of events from e^+p interactions with $Q^2 \lesssim 4$ GeV 2 and a median of $Q^2 \approx 10^{-3}$ GeV 2 . The events are restricted to the kinematic range $134 < W < 277$ GeV using the procedure described in Section 5.

An iterative cone algorithm in the $\eta - \varphi$ plane [19, 20] is used to reconstruct jets from the energy measured in the CAL cells. A detailed description of the algorithm can be found in [17]. The jets reconstructed from the CAL cell energies are called *cal* jets and the variables associated with them are denoted by $E_{T,cal}^{jet}$, η_{cal}^{jet} and φ_{cal}^{jet} . The axis of the jet is defined according to the Snowmass convention [20], where η_{cal}^{jet} (φ_{cal}^{jet}) is the transverse-energy weighted mean pseudorapidity (azimuth) of all the CAL cells belonging to that jet. Events with at least one jet satisfying $E_{T,cal}^{jet} > 10$ GeV and $-1 < \eta_{cal}^{jet} < 2$ are retained. Three samples of jets have been selected depending on the cone radius used in the jet search: 18897 jets for $R = 1.0$, 11197 jets for $R = 0.7$ and 7070 jets for $R = 0.5$. The only significant remaining background is from unidentified DIS neutral current interactions with $Q^2 > 4$ GeV 2 , which is estimated using Monte Carlo techniques to be below 2%.

4 Monte Carlo simulation

Samples of events were generated using Monte Carlo (MC) simulations to determine the response of the detector to jets of hadrons and the correction factors for the inclusive jet cross sections.

The programs PYTHIA 5.7 [21] and HERWIG 5.8 [22] were used to generate photoproduction events for resolved and direct processes. In PYTHIA the positron-photon vertex was modelled according to the Weizsäcker-Williams approximation. In the case of HERWIG, the exact matrix elements were used for direct processes ($e^+g \rightarrow e^+q\bar{q}$ and $e^+q \rightarrow e^+qg$) and the equivalent photon approximation for resolved processes. Events were generated using GRV-HO [13] for the photon parton distributions and MRSA [23] for the proton parton distributions. In addition, samples of events using the LAC1 parametrisation [24] for the photon parton distributions were considered. In both generators, the partonic processes were simulated using LO matrix elements, with the inclusion of initial and final state parton showers. Fragmentation into hadrons was performed using the LUND [25] string model as implemented in JETSET [26] in the case of PYTHIA, and the cluster model [27] in the case of HERWIG. Samples of events were generated with different values of the cut-off on the transverse momentum of the two outgoing partons starting at $\hat{p}_{Tmin} = 8$ GeV. For the measurements presented in this paper, the events generated using the PYTHIA and HERWIG programs have been used for calculating energy corrections and for correcting the data for detector and acceptance effects. The corrections provided by the PYTHIA generator have been used as default values and the ones given by the HERWIG generator have been used to estimate the systematic errors coming from the fragmentation model.

Additional samples of events were generated using the option of multiparton interactions (MI) in PYTHIA. This option, which applies only to resolved processes, adds interactions between the partons in the proton and the photon remnants to the hard scattering process of the event. These multiparton interactions are calculated as LO QCD processes and give an estimation of the underlying event. The PYTHIA MI events were generated with a cut-off for the effective minimum transverse momentum for multiparton interactions of 1 GeV [17] and with a cut-off on the transverse momentum of the two outgoing partons from the hard scattering of $\hat{p}_{Tmin} = 8$ GeV.

All generated events were passed through the ZEUS detector and trigger simulation programs [16]. They were reconstructed and analysed by the same program chain as the data.

For the Monte Carlo events, the jet search is performed from the energy measured in the CAL cells in the same way as in the data. The same jet algorithm is also applied to the final state particles. In this search, all particles with lifetimes longer than 10^{-13} s and with polar angles between 5° and 175° are considered. The jets found are called *hadron* jets and the variables associated with them are denoted by $E_{T,had}^{jet}$, η_{had}^{jet} and φ_{had}^{jet} . *Hadron* jets with $E_{T,had}^{jet} > 14$ GeV and $-1 < \eta_{had}^{jet} < 2$ are selected.

5 Energy corrections

The fivefold increase in statistics in 1994 allowed the CAL energy scale to be studied in more detail than in ref. [4]. The comparison of the energy measured in the central region of the CAL to the momentum measured in the tracking system for the scattered positron in neutral current DIS events, and the transverse momentum balance in neutral current DIS events, showed a $(6 \pm 3)\%$ difference between data and MC [28]. This 6% disagreement has been corrected for

in the present analysis. In the analysis of the 1993 data, the possibility of such a discrepancy was allowed for in the systematic uncertainties.

Particles impinging on the CAL lose energy in the inactive material in front of the CAL. The inactive material constitutes about one radiation length except in the region around the rear beampipe, $\theta \gtrsim 170^\circ$, and the support structures, $25^\circ \lesssim \theta \lesssim 45^\circ$ and $130^\circ \lesssim \theta \lesssim 145^\circ$, where it reaches 2.5 radiation lengths. For the measurements presented here, the transverse energy of the jets has also been corrected for these energy losses as explained below.

The comparison of the reconstructed jet variables between the *hadron* and the *cal* jets in simulated events shows no significant systematic shift in the angular variables η_{cal}^{jet} and φ_{cal}^{jet} with respect to η_{had}^{jet} and φ_{had}^{jet} . Therefore, no correction is needed for η^{jet} and φ^{jet} ($\eta^{jet} \approx \eta_{cal}^{jet}$ and $\varphi^{jet} \approx \varphi_{cal}^{jet}$). However, the transverse energy of the *cal* jet underestimates that of the *hadron* jet by an average amount of 16% with an r.m.s. of 11%. The transverse energy corrections to *cal* jets averaged over the azimuthal angle were determined using the MC events. These corrections are constructed as multiplicative factors, $C(E_{T,cal}^{jet}, \eta_{cal}^{jet})$, which, when applied to the E_T of the *cal* jets provide the ‘corrected’ transverse energies of the jets, $E_T^{jet} = C(E_{T,cal}^{jet}, \eta_{cal}^{jet}) \times E_{T,cal}^{jet}$.

The method of Jacquet-Blondel [29], applied to the photoproduction regime [30], is used to estimate W from the energies measured in the CAL cells: $W^{cal} = \sqrt{2E_p \cdot (E - p_Z)}$, where E is the total CAL energy and p_Z is the Z component of the directed energy measured in the CAL cells. Due to energy lost in the inactive material in front of the CAL and to particles lost in the rear beampipe, W^{cal} systematically underestimates W by approximately 10% with an r.m.s. of 5%. This effect is adequately reproduced by the MC simulation of the detector. To compensate for this underestimation, MC samples of events were used to determine a correction procedure to W^{cal} as a function of W^{cal} and of the pseudorapidity of the most backward jet in the event (η_{min}^{jet}). This correction has been constructed as a multiplicative function, $Y(W^{cal}, \eta_{min}^{jet})$, in a similar way as the correction to the jet transverse energy. When applying the function Y to W^{cal} , $W = Y(W^{cal}, \eta_{min}^{jet}) \times W^{cal}$, the corrected γp centre-of-mass energy is obtained, and events with $134 < W < 277$ GeV are retained.

The response of the CAL to jets has been checked by the following procedure [31]. In the central region ($|\eta^{jet}| < 1$), the multiplicity distribution and the p_T -spectrum of charged particles within the *cal* jets have been compared for data and Monte Carlo samples using the reconstructed tracks. The tracks were required to be in the ranges $|\eta^{track}| < 1.5$ and $p_T^{track} > 300$ MeV, where p_T^{track} is the transverse momentum of the track with respect to the beam axis. Tracks were associated with a *cal* jet when the extrapolated trajectory reached the CAL within the cone of the *cal* jet. PYTHIA describes well all the measured distributions. In this η^{jet} region, the momenta of the tracks in the *cal* jet are used to determine the total transverse energy carried by the charged particles, $E_{T,tracks}^{jet}$. Then, the ratio $r_{tracks} \equiv E_{T,tracks}^{jet}/E_{T,cal}^{jet}$ is formed, and the distributions of this ratio for the inclusive *cal* jet sample with $R = 1.0$ in data and simulations are compared, as shown in Figure 1a. The mean value of the distribution in r_{tracks} has been determined as a function of η^{jet} for data ($\langle r_{tracks} \rangle_{data}$) and simulations ($\langle r_{tracks} \rangle_{MC}$). From the values of the quantity $(\langle r_{tracks} \rangle_{data} / \langle r_{tracks} \rangle_{MC}) - 1$, shown in Figure 1c (circles), we conclude that the energy scale of the jets with $|\eta^{jet}| < 1$ is correct to within $\pm 3\%$.

In the forward region, $1 < \eta^{jet} < 2$, the energy scale of the jets is studied using the transverse energy imbalance in dijet events with one jet in the central region and the other in the forward region. The distributions of the ratio $r_{dijet} \equiv E_{T,cal}^{jet}(\text{forward jet})/E_{T,cal}^{jet}(\text{central jet})$ in data and simulations are compared in Figure 1b. The values of the quantity $(\langle r_{dijet} \rangle_{data} / \langle r_{dijet} \rangle_{MC}) - 1$ (see Figure 1c, square symbols) show that in the forward region the energy scale of the jets is

also correct to within $\pm 3\%$.

It is noted that since the widths of the r_{tracks} and r_{dijet} distributions in the data are reasonably well described by the PYTHIA simulations, the resolution in the energy of the jets is also correctly described.

This procedure has been also applied to the inclusive *cal* jet sample with $R = 0.7$ and leads to the same conclusions. The use of HERWIG instead of PYTHIA gives similar results. Therefore, a $\pm 3\%$ uncertainty on the energy scale of the jets is included as a systematic variation in the present analysis.

6 Jet profiles

The presence of energy not associated to the hard-scattering process (the ‘underlying event’) in the data has been investigated through the study of the transverse energy flow around the jet axis both inside and outside of the jet cone.

The transverse energy profile around the jet axis was measured using the energies and angles of the CAL cells uncorrected for detector effects. The distribution of transverse energy in the hemisphere of the jet, as a function of $\Delta\eta \equiv \eta_{cell} - \eta^{jet}$ and integrated over $|\Delta\varphi| \equiv |\varphi_{cell} - \varphi^{jet}| < \pi/2$, is shown in Figures 2 and 3 for the inclusive jet data samples ($R = 1.0$ and 0.7) in three η^{jet} ranges and two E_T^{jet} regions². The data exhibit a pronounced peak at $\Delta\eta = 0$ and an asymmetric pedestal. The height of the peak increases as E_T^{jet} increases. As a function of η^{jet} , it is fairly constant in the region $-1 < \eta^{jet} < 1$ and decreases in the region $\eta^{jet} > 1$; this decrease is most significant for jets with $R = 1.0$. The height of the pedestal for $\Delta\eta > 1$ (proton side) slightly increases with increasing η^{jet} , the effect being more pronounced for $R = 1.0$ and low E_T^{jet} .

The expectations from PYTHIA simulations including resolved plus direct processes are compared to the data in Figures 2 and 3. The transverse energy profile in the data is well described by the simulations of PYTHIA except for jets with $\eta^{jet} > 1$ and lowest E_T^{jet} ($E_T^{jet} \approx 14$ GeV). In this region, an excess of transverse energy outside of the jet cone with respect to PYTHIA simulations is observed [3,4,5,32]. The excess is reduced for jets defined with $R = 0.7$ in comparison to jets defined with $R = 1.0$ (see Figure 2). In order to simulate an increased energy flow, the PYTHIA MI generator is used, which gives rise to energy not associated with the hard-scattering process. PYTHIA MI gives an improved description of the data for forward low- E_T^{jet} jets with $R = 1.0$, but lies above the data for $\eta^{jet} < 1$ in the case of $R = 1.0$ and in all η^{jet} ranges for $R = 0.7$. For jets with $E_T^{jet} > 21$ GeV, no significant discrepancies are observed between data and PYTHIA simulations with or without multiparton interactions (see Figure 3).

The internal structure of the jets may be investigated using the jet shape, defined as the average fraction of the jet transverse energy that occurs inside an inner cone concentric with the jet defining cone [14]. The shape of jets selected using $R = 1.0$ has been recently measured in photoproduction at HERA [17] and found to be well described by the PYTHIA calculations except for the inclusive production of jets with $\eta^{jet} > 1$ and low E_T^{jet} (14 GeV $< E_T^{jet} < 17$ GeV). We have performed the same type of analysis for jets with $R = 0.7$ and, in this case, the measured jet shapes (not shown) are well described by the PYTHIA (with or without multiparton interactions) calculations in the entire η^{jet} region.

²The decrease of the $\Delta\eta$ distribution seen both in data and the simulations in the region $\Delta\eta > 2$ for the forward jets ($1 < \eta^{jet} < 2$) is a geometric effect: the most forward edge of the CAL is at $\eta = 4.3$.

These observations indicate that the uncertainties on the jet measurements due to possible underlying event contributions become reduced at high E_T^{jet} ($E_T^{jet} > 21$ GeV) or when using a reduced cone radius ($R = 0.7$).

7 Acceptance corrections and systematic uncertainties

The MC generated event samples of resolved and direct processes were used to compute the acceptance corrections to the inclusive jet distributions. These correction factors take into account the efficiency of the trigger, the selection criteria and the purity and efficiency of the jet reconstruction. The differential cross sections $d\sigma/d\eta^{jet}$ are then obtained by applying bin-by-bin corrections to the measured jet distributions. The predictions of the generators PYTHIA and HERWIG for the uncorrected distributions were compared to the data for several choices of the parton densities in the photon and proton and for various combinations of resolved and direct processes. A good description of the η^{jet} data distributions is obtained by the MC except for forward low- E_T^{jet} jets with $R = 1.0$. The bin-by-bin correction factors lie between 0.7 and 1.4 depending on η^{jet} , E_T^{jet} threshold and W region considered. The dominant effect arises from migrations over the E_T^{jet} threshold.

A detailed study of the sources contributing to the systematic uncertainties of the measurements has been performed. The study of the systematic uncertainties includes (a typical value for each item is indicated):

- Use of the HERWIG generator to evaluate the energy corrections to *cal* jets and the correction factors to the observed inclusive jet distributions. The effect of this variation is typically within $\pm 5\%$ in the region $0.5 < \eta^{jet} < 2$ and increases to $\approx 10\%$ for $\eta^{jet} < 0.5$.
- Uncertainties in the simulation of the trigger and the variation of the cuts used to select the data within the ranges allowed by the comparison between data and MC simulations ($\approx 5\%$).
- Use of the PYTHIA generator including multiparton interactions in resolved processes to evaluate the energy corrections to *cal* jets and the correction factors to the observed inclusive jet distributions ($\approx 3\%$). In the region of forward low- E_T^{jet} jets with $R = 1.0$, an improved description of the data is obtained by using PYTHIA MI.
- Choice of different parton densities in the photon (GRV-HO and LAC1) for the generation of the PYTHIA MC samples ($\approx 2\%$).

All these systematic uncertainties have been added in quadrature to the statistical errors and are shown as thin error bars in the figures.

- The absolute energy scale of the *cal* jets in simulated events has been varied by $\pm 3\%$ for the reasons discussed in Section 5. The effect of this variation on the inclusive jet cross sections is $\approx \pm 12\%$ in the region $0 < \eta^{jet} < 2$, and increases up to $\approx 35\%$ for $\eta^{jet} \approx -1$. This uncertainty represents the dominant source of systematic error and is highly correlated between measurements at different η^{jet} points. It is shown as a shaded band in each figure.

In addition, there is an overall normalisation uncertainty of 1.5% from the luminosity determination, which is not included.

8 Results

8.1 Differential cross sections

We present measurements of inclusive differential jet cross sections for the reaction

$$e^+p \rightarrow e^+ + \text{jet} + X$$

in the kinematic region defined by $Q^2 \leq 4 \text{ GeV}^2$ and $134 < W < 277 \text{ GeV}$. These cross sections refer to jets at the hadron level with cone radii of $R = 1.0$ and 0.7 units in the $\eta - \varphi$ plane. The cross section $d\sigma/d\eta^{jet}$ has been measured in the η^{jet} range between -1 and 2 integrated above E_T^{jet} from four different thresholds ($E_T^{jet} > 14, 17, 21$ and 25 GeV). The cross section $d\sigma/d\eta^{jet}$ for $E_T^{jet} > 14 \text{ GeV}$ has also been measured for three different regions of W : $134 < W < 190 \text{ GeV}$, $190 < W < 233 \text{ GeV}$ and $233 < W < 277 \text{ GeV}$. The results are presented in Figures 4 to 7 and in Tables 1 to 4.

For $E_T^{jet} > 14$ and 17 GeV , the behaviour of the cross section as a function of η^{jet} in the region $\eta^{jet} > 1$ is very different for $R = 1.0$ and $R = 0.7$ (see Figures 4 and 5): it is constant for $R = 1.0$ whereas it decreases as η^{jet} increases for $R = 0.7$. On the other hand, the behaviour for $E_T^{jet} > 21$ and 25 GeV is approximately the same in both $R = 1.0$ and 0.7 cases. There are two effects which contribute to the observed differences in the region $\eta^{jet} > 1$ for $E_T^{jet} > 14$ and 17 GeV : a) the jets become broader as η^{jet} (E_T^{jet}) increases (decreases) [17] and, b) the pedestal in the jet profile is integrated over approximately half the area for jets with $R = 0.7$. In addition, the height of the pedestal (see Section 6) is larger for forward jets with $R = 1.0$. Therefore, the differences between the cross sections for the two radii can be attributed to the fact that the use of $R = 0.7$ selects more collimated jets and suppresses the underlying event contribution.

The results for $d\sigma/d\eta^{jet}$ in different regions of W for $E_T^{jet} > 14 \text{ GeV}$ and with $R = 1.0$ ($R = 0.7$) are presented in Figure 6 (7). For $R = 1.0$, the cross section increases with increasing values of η^{jet} and is constant in the high η^{jet} region, whereas for $R = 0.7$ the cross section decreases as η^{jet} increases in the high η^{jet} region. For increasing values of W the maximum of the cross section with $R = 1.0$ ($R = 0.7$) shifts to lower values of η^{jet} . As the energy of the incoming quasi-real photon increases, W increases and the events are boosted more backwards in the laboratory frame.

8.2 Comparison to NLO calculations

NLO QCD calculations of $d\sigma/d\eta^{jet}$ [9, 10] are compared to our measurements in Figures 4 to 7. These predictions include resolved and direct processes. The CTEQ4M [33] proton parton densities have been used. For the photon parton distributions, the AFG [34], GRV-HO [13] and GS96 [35] parametrisations have been used³. In the calculations shown here, the renormalisation and factorisation scales have been chosen equal to E_T^{jet} and α_s was calculated at two loops with $\Lambda_{\overline{MS}}^{(4)} = 296 \text{ MeV}$ [9].

The comparison of the data with NLO calculations is subject to the uncertainty in matching the experimental and theoretical jet algorithms. Since the calculations include only up to three partons in the final state, the maximum number of partons in a single jet is two. Therefore, the overlapping and merging effects of the experimental jet algorithm are not reproduced in the

³The calculations using GRV-HO or GS96 are from [9] and those using AFG from [10]. For the same photon parton distributions, the calculations from [9] and [10] differ typically by less than $\pm 5\%$.

theoretical calculation [14, 36]. An attempt was made to simulate these effects by introducing an ad-hoc R_{SEP} parameter [14]: two partons are not merged into a single jet if their separation in the $\eta - \varphi$ plane is more than R_{SEP} . The calculations of the cross sections shown in Figures 4 to 7 have been made for $R_{SEP} = R$. In addition, the calculations using GS96 and $R_{SEP} = 2R$ are also shown. The spread of the calculations using GS96 for $R_{SEP} = R$ and $R_{SEP} = 2R$ indicates the magnitude of the theoretical uncertainty due to these effects.

As discussed above, the NLO calculations refer to jets built out of at most two partons whereas the measurements refer to jets at the hadron level. An estimate of the effects of hadronisation has been obtained by comparing the cross sections for jets of hadrons and jets of partons calculated with the PYTHIA generator. The ratio of $(d\sigma/d\eta^{jet}[\text{hadrons}])/(d\sigma/d\eta^{jet}[\text{partons}])$ for jets with $R = 1.0$ ($R = 0.7$) is relatively constant as a function of η^{jet} and within approximately 10% (20%) of unity. Due to the approximations used in the MC simulations, these estimations are not to be taken as corrections to the parton level for the measurements presented here.

The NLO calculations give a good description of the measured differential cross sections in magnitude and shape for $E_T^{jet} > 21$ and 25 GeV for both cone radii $R = 1.0$ and 0.7. For $E_T^{jet} > 14$ GeV, the behaviour of the measured cross sections is different for $R = 1.0$ and 0.7, whereas the calculations exhibit the same shape for both radii. For $R = 1.0$, the shape of the cross section is well described for $-1 < \eta^{jet} < 0.5$. For higher values of η^{jet} , the measured cross section is constant, as discussed in Section 8.1, whereas the theoretical curves decrease. These differences are not present when $R = 0.7$ is used: the NLO calculations describe well the magnitude and shape of the measured differential cross sections with $R = 0.7$ for all E_T^{jet} thresholds in the entire range of η^{jet} .

The measured differential cross sections in ranges of W for $R = 1.0$ and $E_T^{jet} > 14$ GeV are reasonably well described for low values of η^{jet} , whereas the NLO calculations fail to describe the high η^{jet} region. The excess of the measured cross section with respect to the calculations increases with increasing W . On the other hand, the measured differential cross sections in bins of W are reasonably well described by the NLO calculations using $R = 0.7$ in the entire region of η^{jet} .

The failure of the NLO calculations to describe the measured cross section for forward low- E_T^{jet} jets with $R = 1.0$ may be due to the following effects: a) the uncertainty due to the choice of renormalisation and factorisation scales is larger than in the case $R = 0.7$ (see next section), and b) non-perturbative contributions like that of the underlying event, which is reduced for jets with $R = 0.7$, are not included. On the other hand, for jets defined with $R = 0.7$ the measured cross sections are well described by the calculations and the uncertainties on the measurements are comparable to the spread of the predictions using different parametrisations of the photon parton distributions.

8.3 Cone radius dependence of the cross section

The cone radius dependence of the inclusive jet cross section, $\sigma(R)$, has been studied. Measurements have been performed of the inclusive jet cross section integrated above $E_T^{jet} > 21$ GeV and $-0.5 < \eta^{jet} < 2$ for three different cone radii ($R = 1.0, 0.7$ and 0.5). These cross sections are given in the same Q^2 and W kinematic region as the measurements presented in Section 8.1. As observed in the jet profiles (see Section 6), the uncertainties on the jet cross sections due to a possible underlying event become reduced at $E_T^{jet} > 21$ GeV. The results for $\sigma(R)$ are presented in Figure 8 and Table 5. The measured cross section is consistent with a linear variation with

R in the range between 0.5 and 1.0.

The results of LO and NLO QCD calculations of $\sigma(R)$ [9], which are performed at the parton level, for different values of the renormalisation and factorisation scales μ are shown in the inset of Figure 8. The LO and NLO GS96 (CTEQ4) sets of photon (proton) parton densities have been used. The LO predictions do not depend on R since there is only one parton per jet and show a large variation with μ . NLO calculations give the lowest-non-trivial order R -dependent contributions to the jet cross section and the μ dependence is largely reduced. However, at small (large) values of R , the NLO predictions for $\sigma(R)$ become a monotonically increasing (decreasing) function of μ . The calculations are most stable for $R \approx 0.5 - 0.7$, consistent with the conclusions of [14]. The uncertainty on the predicted cross section due to the choice of μ , estimated by changing μ from $E_T^{jet}/4$ to E_T^{jet} , is 5% (20%) at $R = 0.7$ ($R = 1.0$).

The slope of $\sigma(R)$ depends on the choice of μ , and is largest (smallest) for small (large) values of μ (see inset of Figure 8). The slope of $\sigma(R)$ in the NLO calculation with $\mu = E_T^{jet}/4$ is closest to that of the measured cross section. In addition to the uncertainty coming from the choice of μ , the predictions are affected by the value of R_{SEP} . QCD calculations with $\mu = E_T^{jet}/4$ and for two values of R_{SEP} , $R_{SEP} = R$ and $2R$, are compared to the measurements in Figure 8. Since the LO predictions of the inclusive jet cross section do not depend on R , the data show the need for QCD corrections. The NLO calculations are consistent with the data within the theoretical and experimental uncertainties, both of which are at the 20% level.

9 Summary and conclusions

Measurements of differential cross sections for inclusive jet photoproduction in e^+p collisions at HERA using the data collected by ZEUS have been presented. The cross sections refer to jets at the hadron level found with an iterative cone algorithm in the $\eta - \varphi$ plane. Measurements of the jet cross sections with two different cone radii, $R = 1.0$ and 0.7 , have been performed. These cross sections are given in the kinematic region defined by $Q^2 \leq 4 \text{ GeV}^2$ and $134 < W < 277 \text{ GeV}$.

A comparison has been made of the transverse energy profiles around the jet axis between data and the leading-logarithm parton-shower simulations of PYTHIA. Requiring high E_T^{jet} ($E_T^{jet} > 21 \text{ GeV}$) or using a cone radius of $R = 0.7$ reduces the discrepancy between data and PYTHIA in the forward region.

NLO QCD calculations [9,10] using currently available parametrisations of the photon parton distributions are compared to the measured cross sections. The uncertainties on the calculations due to the choice of renormalisation and factorisation scales, and non-perturbative effects like the underlying event are smaller for jets with $R = 0.7$ than in the case of $R = 1.0$. The calculations describe the measured cross sections well for jets defined with $R = 1.0$ and 0.7 for $E_T^{jet} > 21$ and 25 GeV . At lower values of E_T^{jet} differences between data and the calculations are seen in the forward region for jets defined with $R = 1.0$. On the other hand, the calculations describe well the measured differential cross sections in the entire range of η^{jet} for jets defined with $R = 0.7$. These conclusions are reinforced when the data are considered in different ranges of W . The uncertainties on the measurements with $R = 0.7$ are comparable to the spread of the predictions using different parametrisations of the photon parton distributions.

The measured cross section for jets with $E_T^{jet} > 21 \text{ GeV}$ and $-0.5 < \eta^{jet} < 2$ is consistent with a linear variation with the cone radius R in the range between 0.5 and 1.0, and shows the need for QCD corrections. The NLO calculations are consistent with the data within the 20% theoretical and experimental uncertainties.

Acknowledgments

We thank the DESY Directorate for their strong support and encouragement. The remarkable achievements of the HERA machine group were essential for the successful completion of this work and are greatly appreciated. We would like to thank B. Harris, M. Klasen, G. Kramer and J. Owens for providing us with their calculations.

References

- [1] J.F. Owens, Phys. Rev. D21 (1980) 54.
- [2] W.J. Stirling and Z. Kunszt, Proceedings of the HERA Workshop (1987) 331; M. Drees and F. Halzen, Phys. Rev. Lett. 61 (1988) 275; M. Drees and R.M. Godbole, Phys. Rev. Lett. 61 (1988) 682 and Phys. Rev. D39 (1989) 169; H. Baer, J. Ohnemus and J.F. Owens, Z. Phys. C42 (1989) 657 and Phys. Rev. D40 (1989) 2844.
- [3] H1 Collab., I. Abt et al., Phys. Lett. B314 (1993) 436.
- [4] ZEUS Collab., M. Derrick et al., Phys. Lett. B342 (1995) 417.
- [5] H1 Collab., T. Ahmed, et al., Nucl. Phys. B445 (1995) 195 and Z. Phys. C70 (1996) 17.
- [6] M. Albrow et al., Proceedings of the 1996 DPF/DPB Summer Study on New Directions for High-Energy Physics (Snowmass 96), Snowmass, Colorado (hep-ph/9706470).
- [7] G. Kramer and S.G. Salesch, Proceedings of the Workshop on Physics at HERA, DESY (1991) 649 and Z. Phys. C61 (1994) 277; L.E. Gordon and J.K. Storrow, Phys. Lett. B291 (1992) 320; D. Bödeker, Phys. Lett. B292 (1992) 164; J.R. Forshaw and R.G. Roberts, Phys. Lett. B319 (1993) 539; M. Greco and A. Vicini, Nucl. Phys. B415 (1994) 386; P. Aurenche, J.P. Guillet and M. Fontannaz, Phys. Lett. B338 (1994) 98; D. Bödeker, G. Kramer and S.G. Salesch, Z. Phys. C63 (1994) 471.
- [8] M. Klasen, G. Kramer and S.G. Salesch, Z. Phys. C68 (1995) 113.
- [9] M. Klasen and G. Kramer, Z. Phys. C76 (1997) 67; M. Klasen, T. Kleinwort and G. Kramer, “Inclusive Jet Production in γp and $\gamma\gamma$ Processes: Direct and Resolved Photon Cross Sections in Next-To-Leading Order QCD”, Preprint DESY 97-234 (hep-ph/9712256); “Photoproduction of Jets at HERA in Next-to-Leading Order QCD”, M. Klasen, Ph.D. thesis, DESY-96-204.
- [10] B.W. Harris and J.F. Owens, Phys. Rev. D56 (1997) 4007, and “Jet Photoproduction and the Structure of the Photon”, FSU-HEP-971020 (hep-ph/9712299).
- [11] S. Frixione and G. Ridolfi, “Jet Photoproduction at HERA”, ETH-TH-97-21 (hep-ph/9707345).
- [12] PLUTO Collab., C. Berger et al., Phys. Lett. B107 (1981) 168, Phys. Lett. B142 (1984) 111, Nucl. Phys. B281 (1987) 365; JADE Collab., W. Bartel et al., Phys. Lett. B121 (1983) 203, Z. Phys. C24 (1984) 231; CELLO Collab., H.-J. Behrend et al., Phys. Lett. B126 (1983) 391; TASSO Collab., M. Althoff et al., Z. Phys. C31 (1986) 527; TPC Collab., H. Aihara et al., Phys. Rev. Lett. 58 (1987) 97, Z. Phys. C34 (1987) 1; AMY Collab., T.

- Sasaki et al., Phys. Lett. B252 (1990) 491, S.K. Sahu et al., Phys. Lett. B346 (1995) 208, T. Kojima et al., Phys. Lett. B400 (1997) 395; TOPAZ Collab., K. Muramatsu et al., Phys. Lett. B332 (1994) 477; OPAL Collab., R. Akers et al., Z. Phys. C61 (1994) 199, K. Ackerstaff et al., Z. Phys. C74 (1997) 33, Phys. Lett. B411 (1997) 387, Phys. Lett. B412 (1997) 225; DELPHI Collab., P. Abreu et al., Z. Phys. C69 (1996) 223.
- [13] M. Glück, E. Reya and A. Vogt, Phys. Rev. D46 (1992) 1973.
- [14] S.D. Ellis, Z. Kunszt and D.E. Soper, Phys. Rev. Lett. 69 (1992) 3615.
- [15] ZEUS Collab., M. Derrick et al., Phys. Lett. B293 (1992) 465.
- [16] The ZEUS Detector, Status Report (1993), DESY 1993.
- [17] ZEUS Collab., J. Breitweg et al., “Measurement of Jet Shapes in Photoproduction at HERA”, DESY 97-191 (hep-ex/9710002), to appear in Eur. Phys. J. C.
- [18] ZEUS Collab., M. Derrick et al., Phys. Lett. B322 (1994) 287.
- [19] CDF Collab., F. Abe et al., Phys. Rev. D45 (1992) 1448.
- [20] J. Huth et al., Proceedings of the 1990 DPF Summer Study on High Energy Physics, Snowmass, Colorado, edited by E.L. Berger (World Scientific, Singapore,1992) p. 134.
- [21] H.-U. Bengtsson and T. Sjöstrand, Comp. Phys. Comm. 46 (1987) 43; T. Sjöstrand, Comp. Phys. Comm. 82 (1994) 74.
- [22] G. Marchesini et al., Comp. Phys. Comm. 67 (1992) 465.
- [23] A.D. Martin, W.J. Stirling and R.G. Roberts, Phys. Rev. D50 (1994) 6734.
- [24] H. Abramowicz, K. Charchuła and A. Levy, Phys. Lett. B269 (1991) 458.
- [25] B. Andersson et al., Phys. Rep. 97 (1983) 31.
- [26] T. Sjöstrand, Comp. Phys. Comm. 39 (1986) 347; T. Sjöstrand and M. Bengtsson, Comp. Phys. Comm. 43 (1987) 367.
- [27] B.R. Webber, Nucl. Phys. B238 (1984) 192.
- [28] ZEUS Collab., M. Derrick et al., Z. Phys. C72 (1996) 399.
- [29] F. Jacquet and A. Blondel in Proceedings of the Study for an ep Facility for Europe, U. Amaldi et al., DESY 79/48 (1979) 377.
- [30] G. D’Agostini and D. Monaldi, Z. Phys. C48 (1990) 467; K.J. Abraham et al., Proceedings of ECFA Workshop on LHC, Aachen (1990) 899; R. van Woudenberg et al., Proceedings of the Workshop on Physics at HERA, DESY (1991) 739.
- [31] C. Glasman, Ph.D. Thesis, Weizmann Institute of Science, DESY-F35D-95-02 (1995); K. Desch, Ph.D. Thesis, Physikalisches Institut der Universität Bonn, BONN-IR-95-13 (1995); Y. Yamazaki, Ph.D. Thesis, Institute for Nuclear Study, University of Tokyo, INS-J-184 (1996).

- [32] ZEUS Collab., M. Derrick et al., Phys. Lett. B348 (1995) 665; ZEUS Collab., J. Breitweg et al., Eur. Phys. J. C1 (1998) 109.
- [33] H.L. Lai et al., Phys. Rev. D55 (1997) 1280.
- [34] P. Aurenche, J.P. Guillet, M. Fontannaz, Z. Phys. C64 (1994) 621.
- [35] L.E. Gordon and J.K. Storrow, Nucl. Phys. B489 (1997) 405.
- [36] W.B. Kilgore and W.T. Giele, Phys. Rev. D55 (1997) 7183.

η^{jet}	$d\sigma/d\eta^{jet} \pm \text{stat.} \pm \text{syst.} \text{ [pb]}$	syst. E_T^{jet} -scale [pb]
	$E_T^{jet} > 14 \text{ GeV}$	
-0.88	$135 \pm 15 \pm 10$	(+50, -30)
-0.62	$345 \pm 25 \pm 90$	(+80, -60)
-0.38	$690 \pm 35 \pm 50$	(+130, -110)
-0.12	$1040 \pm 40 \pm 120$	(+170, -120)
0.12	$1330 \pm 45 \pm 90$	(+190, -150)
0.38	$1535 \pm 45 \pm 170$	(+210, -160)
0.62	$1790 \pm 50 \pm 60$	(+220, -160)
0.88	$1785 \pm 50 \pm 80$	(+200, -160)
1.12	$1715 \pm 50 \pm 110$	(+170, -140)
1.38	$1690 \pm 50 \pm 80$	(+180, -170)
1.62	$1655 \pm 50 \pm 110$	(+230, -150)
1.88	$1785 \pm 50 \pm 100$	(+220, -210)
	$E_T^{jet} > 17 \text{ GeV}$	
-0.62	$80 \pm 10 \pm 10$	(+30, -20)
-0.38	$185 \pm 15 \pm 30$	(+50, -40)
-0.12	$355 \pm 25 \pm 30$	(+70, -50)
0.12	$500 \pm 25 \pm 30$	(+80, -70)
0.38	$625 \pm 30 \pm 50$	(+100, -90)
0.62	$755 \pm 35 \pm 40$	(+100, -70)
0.88	$750 \pm 35 \pm 20$	(+100, -80)
1.12	$725 \pm 35 \pm 50$	(+80, -90)
1.38	$690 \pm 30 \pm 40$	(+90, -70)
1.62	$710 \pm 35 \pm 70$	(+100, -90)
1.88	$665 \pm 30 \pm 30$	(+110, -70)
	$E_T^{jet} > 21 \text{ GeV}$	
-0.25	$50 \pm 5 \pm 15$	(+15, -10)
0.25	$205 \pm 10 \pm 15$	(+35, -35)
0.75	$305 \pm 15 \pm 5$	(+50, -40)
1.25	$280 \pm 15 \pm 20$	(+30, -35)
1.75	$235 \pm 15 \pm 30$	(+35, -35)
	$E_T^{jet} > 25 \text{ GeV}$	
0.25	$70 \pm 5 \pm 5$	(+15, -10)
0.75	$125 \pm 10 \pm 15$	(+20, -20)
1.25	$125 \pm 10 \pm 15$	(+20, -15)
1.75	$120 \pm 10 \pm 10$	(+25, -20)

Table 1: Differential e^+p cross section $d\sigma/d\eta^{jet}$ for inclusive jet production integrated above different E_T^{jet} thresholds in the kinematic region defined by $Q^2 \leq 4 \text{ GeV}^2$ and $134 < W < 277 \text{ GeV}$ for jets with a cone radius $R = 1.0$. The statistical and systematic uncertainties –not associated with the absolute energy scale of the jets– are also indicated. The systematic uncertainties associated to the absolute energy scale of the jets are quoted separately. The overall normalization uncertainty of 1.5% is not included.

η^{jet}	$d\sigma/d\eta^{jet} \pm \text{stat.} \pm \text{syst.} [\text{pb}]$	syst. E_T^{jet} -scale [pb]
	$E_T^{jet} > 14 \text{ GeV}$	
-0.88	$85 \pm 15 \pm 10$	(+30, -20)
-0.62	$260 \pm 20 \pm 60$	(+70, -50)
-0.38	$495 \pm 30 \pm 60$	(+110, -80)
-0.12	$735 \pm 35 \pm 80$	(+120, -90)
0.12	$935 \pm 35 \pm 50$	(+120, -110)
0.38	$1050 \pm 40 \pm 60$	(+130, -120)
0.62	$1225 \pm 40 \pm 60$	(+140, -120)
0.88	$1165 \pm 40 \pm 40$	(+110, -110)
1.12	$1065 \pm 45 \pm 70$	(+120, -110)
1.38	$1055 \pm 40 \pm 30$	(+120, -100)
1.62	$965 \pm 35 \pm 40$	(+110, -100)
1.88	$850 \pm 35 \pm 40$	(+90, -90)
	$E_T^{jet} > 17 \text{ GeV}$	
-0.62	$60 \pm 10 \pm 10$	(+20, -20)
-0.38	$150 \pm 15 \pm 20$	(+30, -30)
-0.12	$240 \pm 20 \pm 30$	(+40, -40)
0.12	$380 \pm 25 \pm 40$	(+60, -50)
0.38	$470 \pm 25 \pm 10$	(+80, -70)
0.62	$525 \pm 25 \pm 20$	(+70, -70)
0.88	$560 \pm 30 \pm 40$	(+70, -70)
1.12	$495 \pm 30 \pm 30$	(+50, -50)
1.38	$465 \pm 25 \pm 30$	(+50, -50)
1.62	$395 \pm 25 \pm 40$	(+50, -40)
1.88	$385 \pm 25 \pm 30$	(+40, -50)
	$E_T^{jet} > 21 \text{ GeV}$	
-0.25	$35 \pm 5 \pm 10$	(+10, -10)
0.25	$160 \pm 10 \pm 5$	(+30, -25)
0.75	$210 \pm 10 \pm 5$	(+30, -25)
1.25	$195 \pm 10 \pm 10$	(+25, -25)
1.75	$170 \pm 10 \pm 20$	(+25, -25)
	$E_T^{jet} > 25 \text{ GeV}$	
0.25	$64 \pm 7 \pm 6$	(+10, -10)
0.75	$93 \pm 8 \pm 11$	(+15, -10)
1.25	$85 \pm 8 \pm 15$	(+15, -10)
1.75	$85 \pm 8 \pm 8$	(+15, -10)

Table 2: Differential e^+p cross section $d\sigma/d\eta^{jet}$ for inclusive jet production integrated above different E_T^{jet} thresholds in the kinematic region defined by $Q^2 \leq 4 \text{ GeV}^2$ and $134 < W < 277 \text{ GeV}$ for jets with a cone radius $R = 0.7$. Other details as in Table 1.

η^{jet}	$d\sigma/d\eta^{jet} \pm \text{stat.} \pm \text{syst.} [\text{pb}]$	syst. E_T^{jet} -scale [pb]
	134 < W < 190 GeV	
0.25	$340 \pm 15 \pm 70$	(+80, -50)
0.75	$720 \pm 25 \pm 60$	(+100, -80)
1.25	$700 \pm 25 \pm 50$	(+80, -70)
1.75	$725 \pm 25 \pm 50$	(+90, -80)
	190 < W < 233 GeV	
-0.25	$305 \pm 15 \pm 60$	(+70, -50)
0.25	$585 \pm 20 \pm 30$	(+70, -60)
0.75	$555 \pm 20 \pm 50$	(+60, -40)
1.25	$495 \pm 20 \pm 30$	(+50, -50)
1.75	$500 \pm 20 \pm 40$	(+70, -50)
	233 < W < 277 GeV	
-0.75	$220 \pm 15 \pm 30$	(+60, -40)
-0.25	$535 \pm 20 \pm 30$	(+80, -60)
0.25	$500 \pm 20 \pm 40$	(+50, -40)
0.75	$495 \pm 20 \pm 30$	(+50, -40)
1.25	$475 \pm 20 \pm 30$	(+50, -40)
1.75	$475 \pm 20 \pm 20$	(+50, -50)

Table 3: Differential e^+p cross section $d\sigma/d\eta^{jet}$ for inclusive jet production integrated above $E_T^{jet} > 14$ GeV in the kinematic region defined by $Q^2 \leq 4$ GeV² and in three regions of W for jets with a cone radius $R = 1.0$. Other details as in Table 1.

η^{jet}	$d\sigma/d\eta^{jet} \pm \text{stat.} \pm \text{syst.} [\text{pb}]$	syst. E_T^{jet} -scale [pb]
$134 < W < 190 \text{ GeV}$		
0.25	$230 \pm 15 \pm 30$	(+50, -40)
0.75	$480 \pm 20 \pm 60$	(+60, -50)
1.25	$450 \pm 20 \pm 30$	(+50, -50)
1.75	$375 \pm 15 \pm 40$	(+50, -40)
$190 < W < 233 \text{ GeV}$		
-0.25	$215 \pm 15 \pm 40$	(+60, -40)
0.25	$400 \pm 20 \pm 10$	(+50, -40)
0.75	$390 \pm 15 \pm 30$	(+40, -30)
1.25	$320 \pm 15 \pm 30$	(+40, -30)
1.75	$270 \pm 15 \pm 20$	(+30, -30)
$233 < W < 277 \text{ GeV}$		
-0.75	$165 \pm 15 \pm 30$	(+50, -30)
-0.25	$385 \pm 15 \pm 30$	(+50, -40)
0.25	$365 \pm 15 \pm 10$	(+40, -40)
0.75	$320 \pm 15 \pm 40$	(+30, -20)
1.25	$285 \pm 15 \pm 10$	(+30, -30)
1.75	$255 \pm 15 \pm 10$	(+20, -30)

Table 4: Differential e^+p cross section $d\sigma/d\eta^{jet}$ for inclusive jet production integrated above $E_T^{jet} > 14 \text{ GeV}$ in the kinematic region defined by $Q^2 \leq 4 \text{ GeV}^2$ and in three regions of W for jets with a cone radius $R = 0.7$. Other details as in Table 1.

Cone radius	$\sigma(R) \pm \text{stat.} \pm \text{syst.} [\text{pb}]$	syst. E_T^{jet} -scale [pb]
$R = 0.5$	$275 \pm 10 \pm 30$	(+40, -30)
$R = 0.7$	$385 \pm 10 \pm 20$	(+60, -50)
$R = 1.0$	$540 \pm 15 \pm 40$	(+90, -80)

Table 5: e^+p cross section $\sigma(R)$ for inclusive jet production integrated above $E_T^{jet} > 21 \text{ GeV}$ and $-0.5 < \eta^{jet} < 2$ in the kinematic region defined by $Q^2 \leq 4 \text{ GeV}^2$ and $134 < W < 277 \text{ GeV}$. Other details as in Table 1.

ZEUS 1994

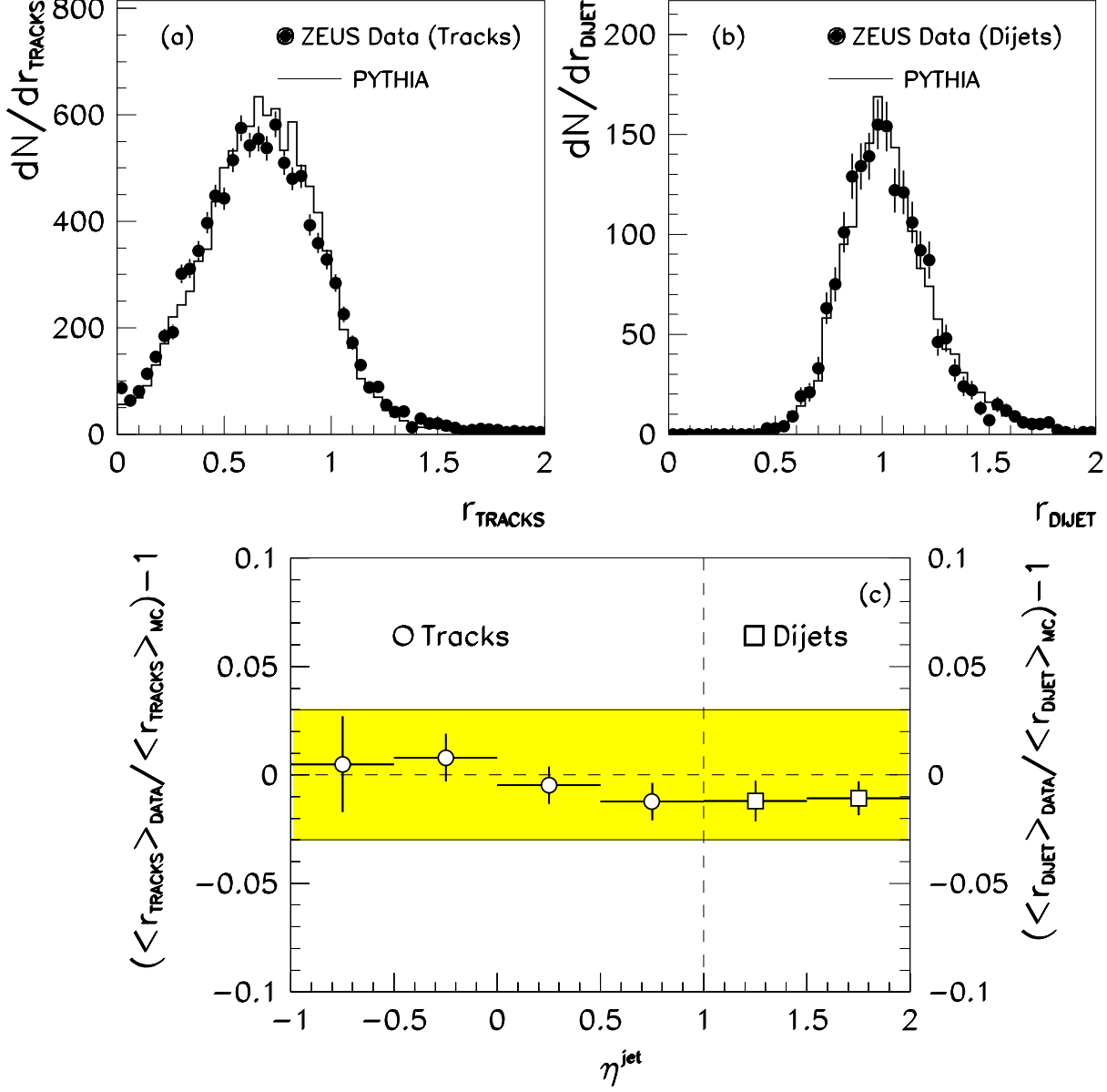


Figure 1: (a) The distribution of $r_{tracks} \equiv E_{T,tracks}^{jet}/E_{T,cal}^{jet}$ for the inclusive jet data sample with $R = 1.0$ (black dots) and as reproduced by the PYTHIA generator and detector simulation (histogram, normalised to the number of jets in the data); (b) the distribution of $r_{dijet} \equiv E_{T,cal}^{jet}(\text{forward})/E_{T,cal}^{jet}(\text{central})$ for the dijet data sample (one jet in the forward region and the other in the central region) with $R = 1.0$ (black dots) and as reproduced by the PYTHIA generator and detector simulation (histogram, normalised to the number of jets in the data); (c) the values of the quantity $(\langle r_{tracks} \rangle_{data} / \langle r_{tracks} \rangle_{MC}) - 1$ (circles) and $(\langle r_{dijet} \rangle_{data} / \langle r_{dijet} \rangle_{MC}) - 1$ (squares). The shaded region displays the band of $\pm 3\%$ around zero.

ZEUS 1994

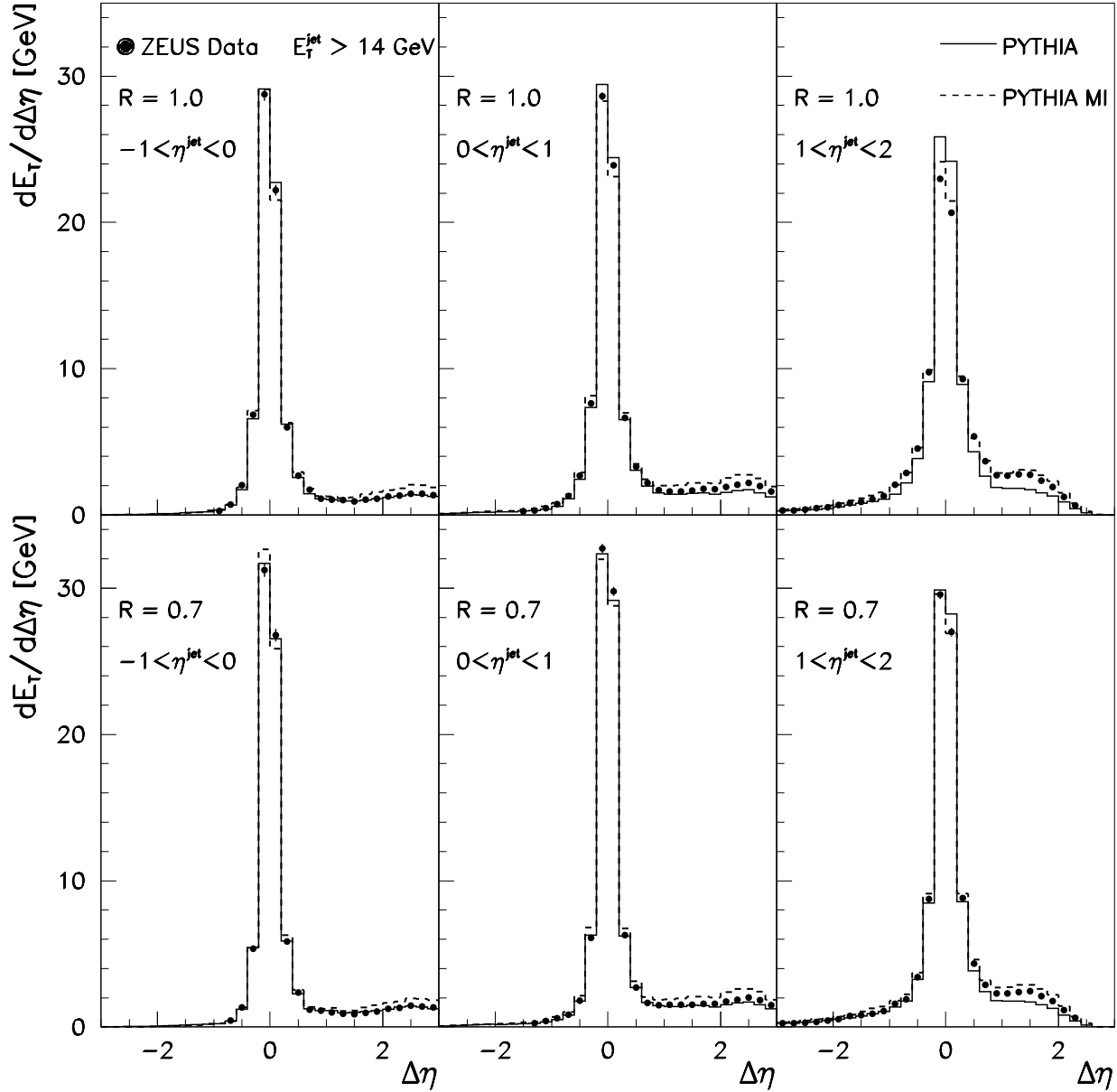


Figure 2: Uncorrected transverse energy profiles for jets with $E_T^{jet} > 14$ GeV and $R = 1.0$ and 0.7 as a function of the distance from the jet axis, $\Delta\eta$ (integrated over $|\Delta\varphi| < \pi/2$), in three η^{jet} regions (black dots). For comparison, PYTHIA and PYTHIA MI simulations including resolved plus direct processes are shown as the solid and dashed histograms, respectively.

ZEUS 1994

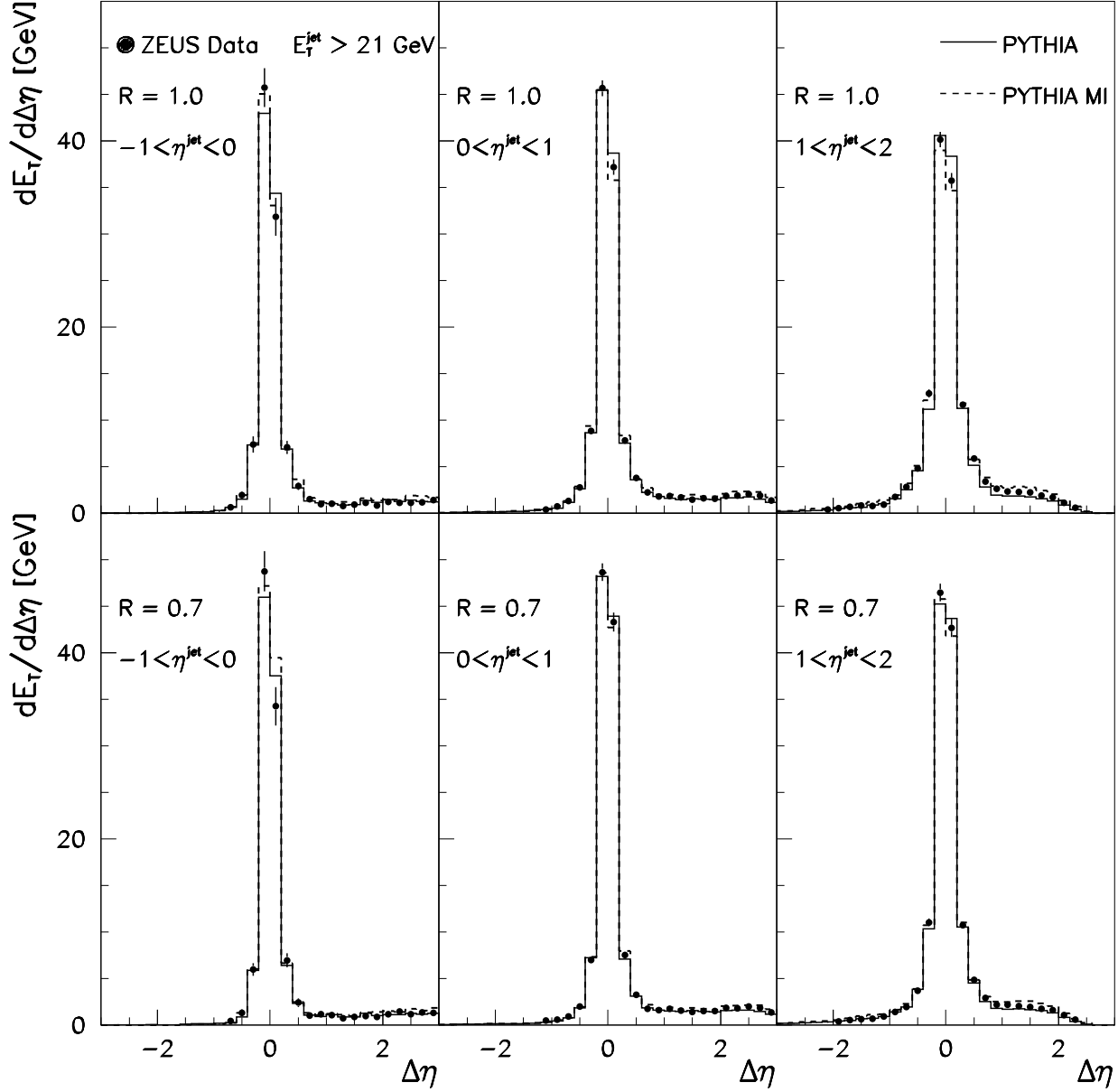


Figure 3: Uncorrected transverse energy profiles for jets with $E_T^{jet} > 21$ GeV and $R = 1.0$ and 0.7 as a function of the distance from the jet axis, $\Delta\eta$ (integrated over $|\Delta\phi| < \pi/2$), in three η^{jet} regions (black dots). For comparison, PYTHIA and PYTHIA MI simulations including resolved plus direct processes are shown as the solid and dashed histograms, respectively.

ZEUS 1994

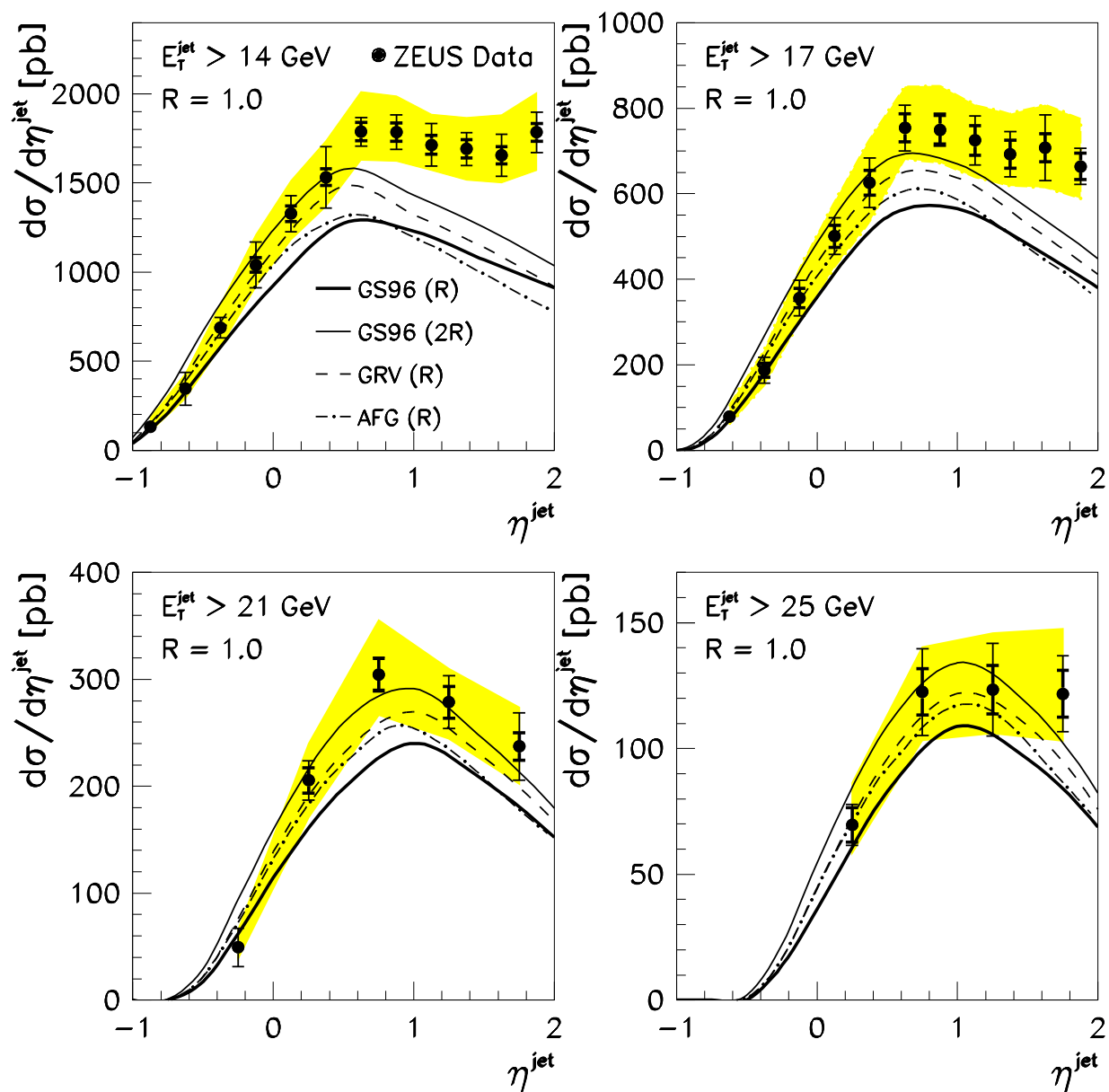


Figure 4: Differential e^+p cross section $d\sigma/d\eta^{\text{jet}}$ for inclusive jet production integrated above E_T^{jet} from four different thresholds ($E_T^{\text{jet}} > 14, 17, 21$ and 25 GeV) in the kinematic region defined by $Q^2 \leq 4$ GeV² and $134 < W < 277$ GeV for jets with a cone radius $R = 1.0$. The thick error bars represent the statistical errors of the data, and the thin error bars show the statistical errors and systematic uncertainties –not associated with the absolute energy scale of the jets– added in quadrature. The shaded bands display the uncertainty due to the absolute energy scale of the jets. For comparison, NLO calculations for three parametrisations of the photon parton distributions, $\mu = E_T^{\text{jet}}$ and for two different values of R_{SEP} are shown: AFG $R_{\text{SEP}} = R$ (dot-dashed line), GRV-HO $R_{\text{SEP}} = R$ (dashed line), GS96 $R_{\text{SEP}} = R$ (thick solid line) and GS96 $R_{\text{SEP}} = 2R$ (thin solid line). The values of R_{SEP} used are indicated in parentheses. In all cases, the CTEQ4M proton parton distributions have been used.

ZEUS 1994

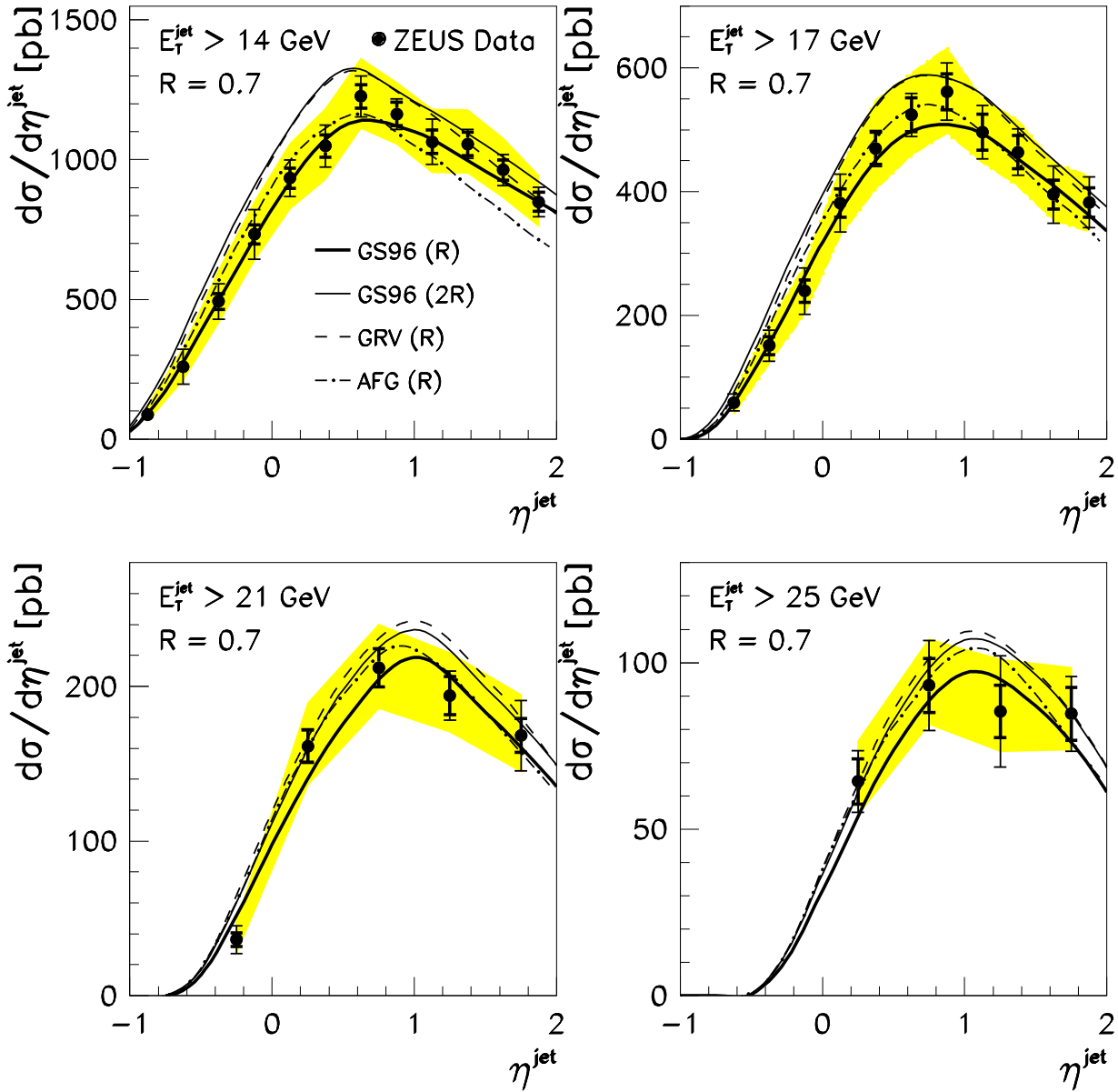


Figure 5: Differential e^+p cross section $d\sigma/d\eta^{\text{jet}}$ for inclusive jet production for jets with a cone radius $R = 0.7$. Other details as in Figure 4.

ZEUS 1994

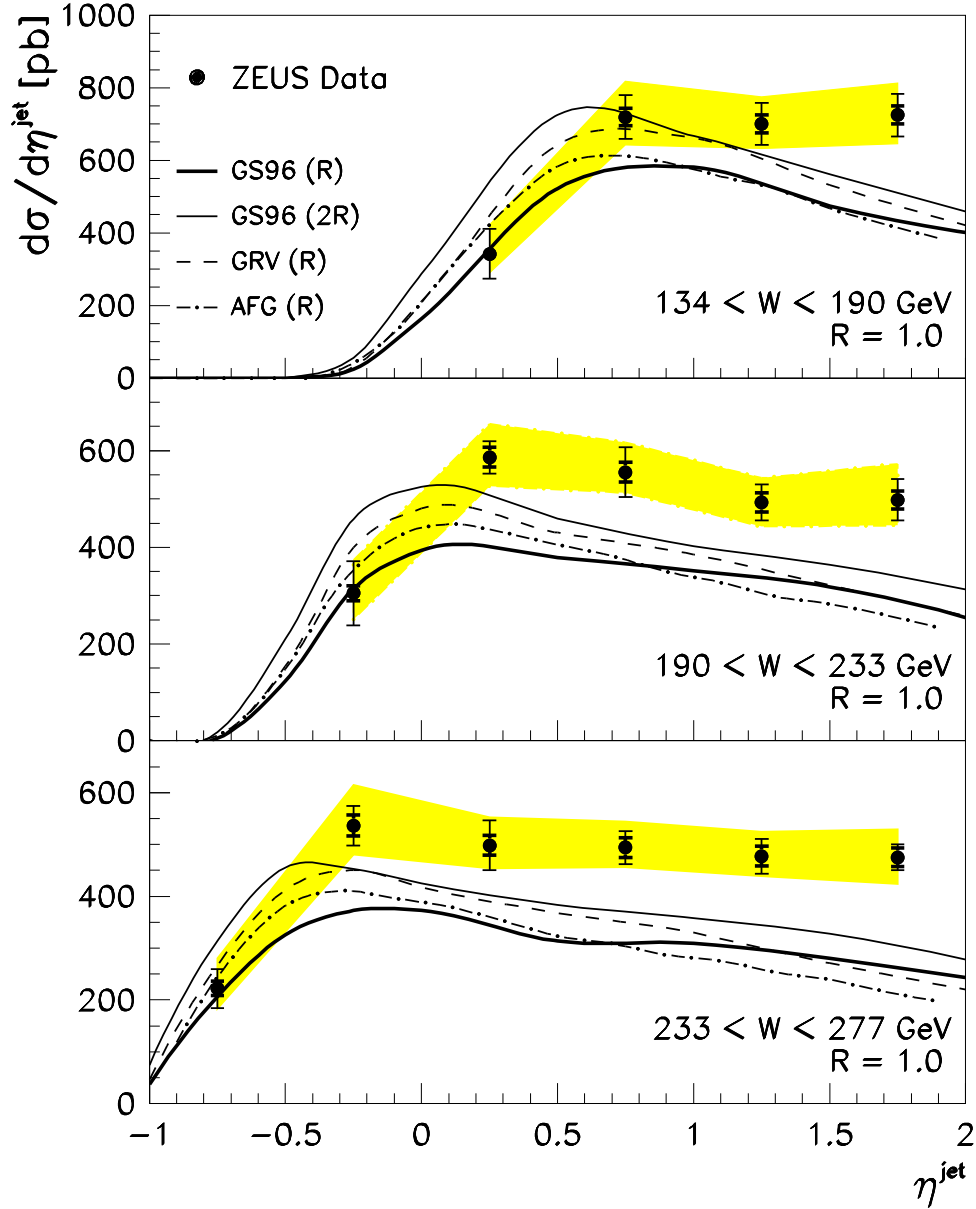


Figure 6: Differential e^+p cross section $d\sigma/d\eta^{\text{jet}}$ for inclusive jet production integrated above $E_T^{\text{jet}} > 14 \text{ GeV}$ in the kinematic region defined by $Q^2 \leq 4 \text{ GeV}^2$ and in three regions of W : $134 < W < 190 \text{ GeV}$ (upper plot), $190 < W < 233 \text{ GeV}$ (middle plot) and $233 < W < 277 \text{ GeV}$ (lower plot) for jets with a cone radius $R = 1.0$. Other details as in Figure 4.

ZEUS 1994

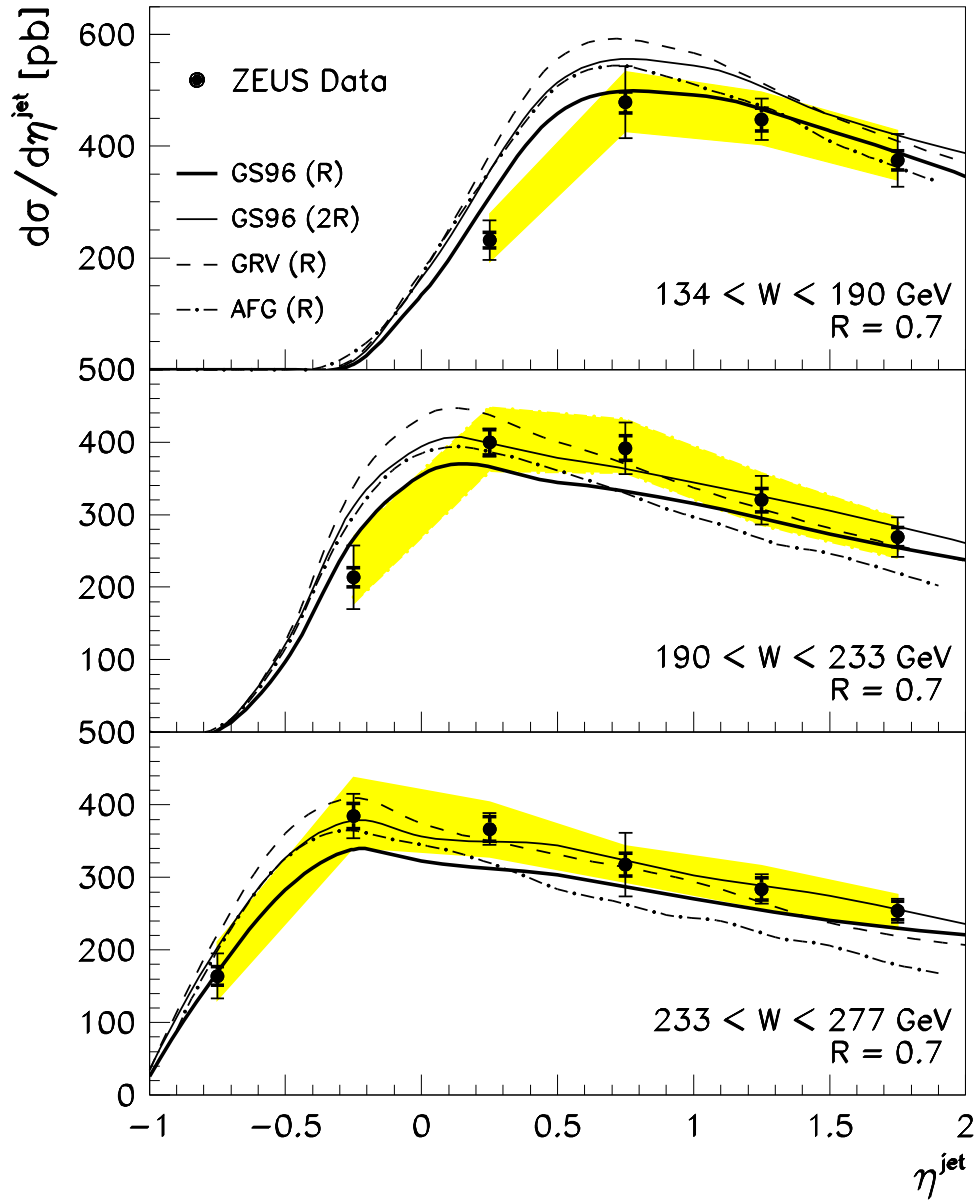


Figure 7: Differential e^+p cross section $d\sigma/d\eta^{\text{jet}}$ for inclusive jet production for jets with a cone radius $R = 0.7$. Other details as in Figure 6.

ZEUS 1994

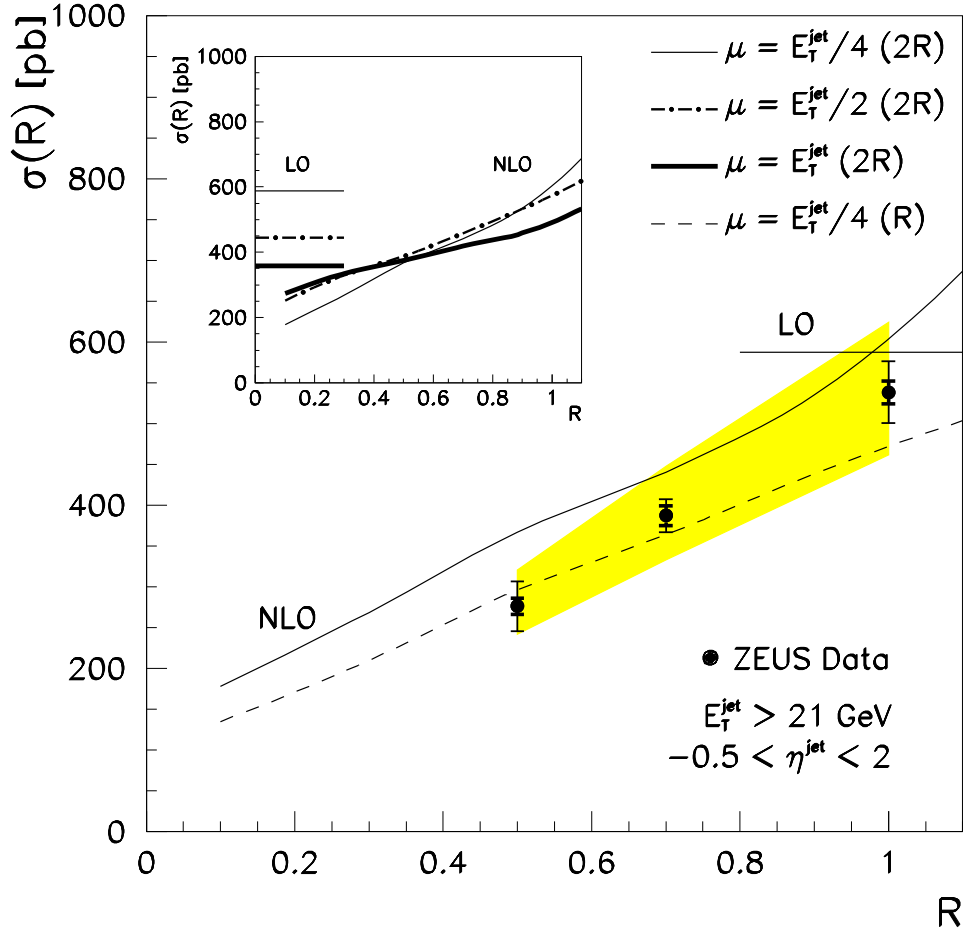


Figure 8: e^+p cross section $\sigma(R)$ as a function of the jet cone radius R for inclusive jet production integrated above $E_T^{jet} > 21$ GeV and $-0.5 < \eta^{jet} < 2$ in the kinematic region defined by $Q^2 \leq 4$ GeV² and $134 < W < 277$ GeV. The thick error bars represent the statistical errors of the data, and the thin error bars show the statistical errors and systematic uncertainties –not associated with the absolute energy scale of the jets– added in quadrature. The shaded band displays the uncertainty due to the absolute energy scale of the jets. LO and NLO calculations using the GS96 (CTEQ4) parametrisations of the photon (proton) parton distributions and $\mu = E_T^{jet}/4$ for two choices of the parameter R_{SEP} are shown. The values of R_{SEP} used are indicated in parentheses. The inset shows the calculations for a fixed value of $R_{SEP} = 2R$ and various choices of μ .